

Available online at www.sciencedirect.com

International Journal of Solids and Structures 44 (2007) 3393–3410

INTERNATIONAL JOURNAL OF
**SOLIDS and
STRUCTURES**www.elsevier.com/locate/ijssolstr

Multi-slip gradient formulation for modeling microstructure effects on shear bands in granular materials

O. Al Hattamleh ^a, B. Muhunthan ^{b,*}, H.M. Zbib ^c^a *Department of Civil Engineering, Hashemite University, P.O. Box 150459, Zarqa 13115, Jordan*^b *Department of Civil and Environmental Engineering, Washington State University, Pullman, WA, USA*^c *School of Mechanical and Materials Engineering, Washington State University, Pullman, WA, USA*

Received 14 March 2006; received in revised form 31 August 2006

Available online 30 September 2006

Abstract

This paper presents a higher order gradient multi-slip formulation to model the effect of inhomogeneous deformation in granular materials. The effects of heterogeneity and porosity anisotropy within the multi-slip formulation are taken into consideration through the modification of the mobilized friction. The mobilized friction is assumed to be a direct function of either the gradient of the porosity distribution or the fabric tensor. The formulation with two active slip planes was implemented into a finite element code and used to simulate biaxial shear tests on dry sand. The analysis quantifies most of the shear band characteristics observed by past experimentation. It is shown that the localization and shear band characteristics in granular materials are very much dependent on the initial fabric and slip system arrangement.

© 2006 Elsevier Ltd. All rights reserved.

Keywords: Dilatancy; Frictional materials; Elastic/plastic; Fabric anisotropy; Shear band; Slip; Gradient deformation

1. Introduction

The mechanical behavior of granular materials is strongly influenced by its microstructure. Porosity is often used to characterize the state of packing in these materials. This scalar measure, however, has been found to be insufficient to characterize their directional behavior and higher order microstructure variables known as “fabric tensors” have been used to describe the distribution and orientation of grains and voids (Oda et al., 1985; Mehrabadi et al., 1982; Tobita, 1989; Pietruszczak and Krucinski, 1989a; Bathurst and Rothenburg, 1990; Muhunthan et al., 1996). Models incorporating these fabric measures are also extant in the literature (Chang and Hicher, 2005; Kachanov and Sevostianov, 2005).

Experiments on various assemblies of discrete particles have shown the overall deformation of a granular mass to consist of simple dilatant shearing deformations on a number of active shearing planes (Oda et al., 1982, 1985; Nemat-Nasser, 2000; Nemat-Nasser and Zhang, 2002). “Double-shearing” plane strain type

* Corresponding author. Tel.: +1 509 335 3921; fax: +1 509 335 7632.

E-mail address: muhuntha@wsu.edu (B. Muhunthan).

constitutive models have been used in the past by many researchers to describe the mechanics of granular materials (Spencer, 1964, 2003; Rudnicki and Rice, 1975; Mehrabadi and Cowin, 1978; Anand, 1983; Zbib, 1991, 1993; Nemat-Nasser and Zhang, 2002). Granular dilatancy has also been incorporated into the double-slip model (Anand and Gu, 2000).

The shear band phenomenon in granular materials has been studied extensively (Roscoe, 1970; Zbib and Aifantis, 1989; de Borst and Muhlhaus, 1992; Vardoulakis, 1996; Oda et al., 1998; Oka et al., 2002; Gajo et al., 2004; Al Hattamleh et al., 2004; Liu et al., 2005). Some of these studies have introduced different higher gradient measures to incorporate microstructure length scale into the classical formulations to model strain localization and shear bands. The performance of higher-order plasticity theories for predicting size effects and localization has been discussed by Engelen et al. (2006).

This paper presents a second order gradient multi-slip plasticity formulation to study strain localization in granular materials. The effects of heterogeneity and anisotropy within the multi-slip formulation are accounted for through the modification of the mobilized friction. The mobilized friction is assumed to be a function of either the gradient of the porosity distribution or the fabric tensor. A two-active slip-plane version of the multi-slip formulation is implemented in ABAQUS (2003) and used to study shear bands and post localization behavior in granular materials.

2. Mathematical preliminaries

The velocity gradient (L_{ij}) of a continuous medium undergoing smooth deformation can be split into two parts; symmetric and skew-symmetric. The symmetric part represents the pure stretching tensor, D_{ij} , and the skew-symmetric part represents the spin tensor, W_{ij} :

$$D_{ij} = \frac{1}{2} (L_{ij} + L_{ij}^T) \quad (1)$$

$$W_{ij} = \frac{1}{2} (L_{ij} - L_{ij}^T) \quad (2)$$

The stretching tensor D_{ij} can be decomposed as:

$$D_{ij} = D_{ij}^e + D_{ij}^p \quad (3)$$

where D_{ij}^e and D_{ij}^p are the elastic and plastic parts, respectively. Similarly, the spin can be written as:

$$W_{ij} = \omega_{ij} + W_{ij}^p \quad (4)$$

where ω_{ij} is the spin of microstructure, and W_{ij}^p the plastic spin.

The equation of equilibrium for quasi-static loading conditions is given by:

$$\sigma_{ij,j} + b_i = 0 \quad (5)$$

where σ_{ij} is the Cauchy stress tensor and b_i is the body force per unit volume. The elastic tensor of stretching D_{ij}^e is assumed to follow Hooke's law:

$$\overset{\circ}{\sigma}_{ij} = C_{ijkl}^e D_{kl}^e \quad (6)$$

$$C_{ijkl}^e = G \left(\delta_{ik} \delta_{jl} + \delta_{il} \delta_{jk} + \frac{2\nu}{1-2\nu} \delta_{ij} \delta_{kl} \right) \quad (7)$$

where C_{ijkl}^e is the elasticity tensor, G the shear modulus, ν the Poisson's ratio, and δ_{ij} the Kronecker delta. The Jaumann rate of Cauchy stress tensor $\overset{\circ}{\sigma}_{ij}$ is defined with respect to the frame rotating with the material as:

$$\overset{\circ}{\sigma}_{ij} = \dot{\sigma}_{ij} - \omega_{ik} \sigma_{kj} + \sigma_{ik} \omega_{kj} \quad (8)$$

3. Multi-slip model for plastic flow

Experiments on various assemblies of discrete particles have shown that the overall deformation of a granular mass consists of sliding and rolling along active shearing planes (Oda et al., 1982, 1985; Nemat-Nasser, 2000). Fig. 1 shows a typical shear plane in a granular material. The deformations along shearing planes are similar to those on slip planes in crystal plasticity where plastic deformation is assumed to take place along well-defined slip directions (Nemat-Nasser, 2000; Anand and Gu, 2000).

In the multi-slip model for soils, plastic deformation is viewed in terms of slips on planes-defined by their normal unit vector n_i and slip direction m_i . Therefore, it is necessary firstly to choose a set of active planes. While in polycrystalline metals, slip systems are uniquely defined; slip planes in soils are not unique. In most cases, these planes have been identified with the slip systems with directions that are symmetrically disposed about the maximum principal stress direction (Mehrabadi and Cowin, 1978; Anand, 1983). However, discrete simulations of granular materials as well as experimental observations have shown that the direction of slip and subsequent plastic deformation is influenced very much by the depositional microstructure.

A typical conjugate slip system for plane strain conditions is as shown in Fig. 2. The components of the slip systems $s^{(1)}$ are given by:

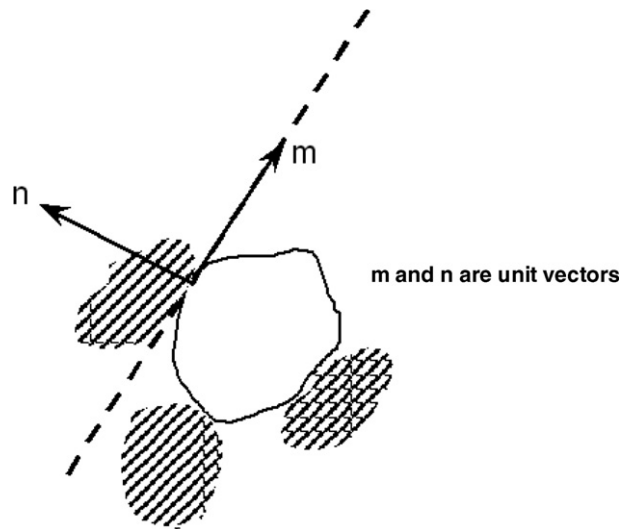


Fig. 1. Schematic representation of dilatant shearing plane.

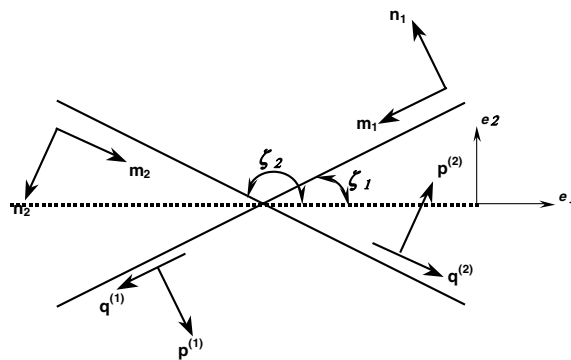


Fig. 2. Typical double-slip system.

$$m_i^{(1)} = -\cos \zeta_1 \cdot e_1 - \sin \zeta_1 \cdot e_2 \quad (9a)$$

$$n_i^{(1)} = -\sin \zeta_1 \cdot e_1 + \cos \zeta_1 \cdot e_2 \quad (9b)$$

where ζ is the angle measured with respect to minor principal stress axis and e_1, e_2 are the unit vectors in the Cartesian coordinate system.

The plastic strain rate tensor consists of simple shearing strain rates $\dot{\gamma}^{p(s)}$ on each of the slip system s , and this shearing is accompanied by shear-induced dilatancy rate $\dot{v}^{(s)}$ in the directions normal to the shear directions:

$$D_{ij}^p = \sum_{s=1}^{s_T} \dot{\gamma}^{p(s)} M_{ij}^{(s)} + \sum_{s=1}^{s_T} \dot{v}^{(s)} N_{ij}^{(s)} \quad (10)$$

$$M_{ij}^{(s)} = (m_i^{(s)} n_j^{(s)} + n_i^{(s)} m_j^{(s)})/2 \quad (10a)$$

$$N_{ij}^{(s)} = n_i^{(s)} n_j^{(s)} \quad (10b)$$

$$W_{ij}^p = \sum_{s=1}^{s_T} \dot{\gamma}^{p(s)} V_{ij}^{(s)} \quad (11)$$

$$V_{ij}^{(s)} = (m_i^{(s)} n_j^{(s)} - n_i^{(s)} m_j^{(s)})/2 \quad (11a)$$

where D_{ij}^p is the plastic strain rate tensor, W_{ij}^p the plastic spin, $\dot{\gamma}^{p(s)} (= \sqrt{\frac{2}{3}} d_{ij}^{p(s)} d_{ij}^{p(s)})$ the effective plastic shear strain rate on the s th slip system, $\dot{v}^{(s)} = \beta \dot{\gamma}^{p(s)}$ the dilatation rate, with β being the *mobilized* dilatancy coefficient and s_T the total number of slip planes. The effective plastic strain is defined by $\gamma^p = \int \dot{\gamma}^p dt$. Moreover, it is assumed that the slip planes are oriented initially at a given angle relative to some plane in space (e.g., the directions of minor principal stresses). This angle is treated as a material parameter and the rotation of the slip line is evaluated as (Asaro, 1979):

$$\dot{m}_i = \omega_{ij} m_j \quad (12a)$$

$$\dot{n}_i = \omega_{ij} n_j \quad (12b)$$

where ω_{ij} is the spin of microstructure as given by Eq. (4).

The total number of independent slip planes depends on the problem under investigation. For three-dimensional deformation of compressible materials, the minimum number of conjugate slip systems is six whereas for incompressible materials it is five. For two-dimensional problems, two slip planes are sufficient (Hirth, 1992).

3.1. Yield functions

The set of yield functions on the slip systems of the granular material is assumed to follow the gradient criterion, $f^{(s)}$:

$$f^{(s)} = q^{(s)} - \mu p^{(s)} - c_1 \nabla^2 \gamma^{p(s)} \quad (13)$$

where $q^{(s)}$ and $p^{(s)}$ are the resolved shear and normal stresses, respectively. They are expressed in terms of the Cauchy stress tensor as:

$$q^{(s)} = \sigma_{ij} : M_{ij}^{(s)} \quad (14)$$

$$p^{(s)} = \sigma_{ij} : N_{ij}^{(s)} \quad (15)$$

c_1 represents the first gradient coefficient and $\nabla^2 \gamma^p$ represents the Laplacian of effective plastic strain. The hardening/softening behavior due to redistribution of contacts is modeled through an evolution law for the *mobilized* friction coefficient, μ (e.g., Zbib and Aifantis, 1989; Vardoulakis, 1996; Anand and Gu, 2000).

The plastic dilatancy for most materials is on the order of the measurement error and can be assumed zero in the absence of phase change and significant void nucleation during plastic deformation. However, dilation

in granular materials is pronounced. The parameter $\dot{\nu}^{(s)} = \beta \dot{\gamma}^{p(s)}$ in Eq. (10) captures induced dilation in the current granular materials model.

3.2. Effective plastic shear strain rate and stiffness tensors

Utilizing the yield and consistency conditions, $f = 0$; $\dot{f} = 0$, along with Eqs. (6), (13), (14) and (15), the effective plastic strain rate can be evaluated as (Al Hattamleh, 2003):

$$\dot{\gamma}^{p(s)} = \frac{\left(M_{ij}^{(s)} + \alpha\mu\delta_{ij}\right) : D_{ij} - c_1 \nabla^2 \dot{\gamma}^{p(s)} / G}{1.0 + |p^{(s)}| h_t / G + \alpha\beta\mu + c'_1 \nabla^2 \gamma^{p(s)} / G} \quad (16)$$

where $h_t = \frac{\partial\mu}{\partial\gamma^p}$, is the strain hardening/softening modulus, $c'_1 = \frac{dc_1}{d\gamma^p}$, $\alpha = K/G$, and K and G are the bulk and shear moduli, respectively. Substituting Eq. (16) into Eq. (6) and combining it with Eq. (10) and letting $c'_1 = 0$ leads to:

$$\overset{a}{\sigma}_{ij} = C_{ijkl} D_{kl} - \overset{a}{\sigma}_{ij}^g \quad (17)$$

$$C_{ijkl} = C_{ijkl}^e - C_{ijkl}^p \quad (17a)$$

$$\overset{a}{\sigma}_{ij}^g = \sum_{s=1}^s c_1 \nabla^2 \dot{\gamma}^{p(s)} \left(M_{ij}^{(s)} + \alpha\beta\delta_{ij}\right) / H^{(s)} \quad (17b)$$

where $H^{(s)} = 1.0 + |p^{(s)}| h_t / G + \alpha\beta\mu$;

The resultant plastic stiffness tensor is given as:

$$C_{ijkl}^p = \frac{G}{H^{(s)}} \left(M_{ik}^{(s)} + \alpha\beta\delta_{ik}\right) \left(M_{jl}^{(s)} + \alpha\mu\delta_{jl}\right) \quad (18)$$

The framework of this model does not involve higher-order stress, and the strain gradient effects come into play via the incremental plastic strain. Therefore, it falls into the strain gradient type framework that preserves the structure of conventional plasticity theories. Thus, the equilibrium equations and boundary conditions are the same as the conventional continuum theories (Shizawa and Zbib, 1999; Huang et al., 2004).

3.3. Friction and dilatancy

The mobilized friction coefficient μ (Eq. (13)) is assumed to be a function of the effective plastic strain:

$$\mu(\gamma^p) = \mu_{cv} + x_1 \left(\gamma^p + \frac{\mu_0 - \mu_{cv}}{x_1}\right) \exp(-x_2 \gamma^p) \quad (19)$$

where μ_{cv} is the internal friction at constant volume, μ_0 the initial mobilized friction, and x_1, x_2 are material parameters determined from experimental results. Similar formulations relating μ to μ_{cv} have been used in the past (Balendran and Nemat-Nasser, 1993a; Anand and Gu, 2000).

Following the work of Taylor (1948) the mobilized dilatancy is expressed as (Vardoulakis, 1996):

$$\beta(\gamma^p) = \mu(\gamma^p) - \mu_{cv} \quad (20)$$

Han and Drescher (1993) have reported some biaxial shear tests on dry sand. A prismatic specimen of 40 mm width, 80 mm length, and 140 mm height was used. The specimen was enclosed between two rigid walls 80 m apart and placed on a platen, which rested on a linear bearing. The linear bearing provided kinematic freedom for the formation of shear bands with the lower portion of the specimen sliding horizontally. The apparatus was placed inside a pressure chamber and the specimen was subjected to a confining pressure and kinematically or statically controlled axial load.

Biaxial tests were performed on coarse, poorly graded Ottawa sand with rounded particles of mean grain diameter $D_{50} = 0.72$ mm. Homogenous dense specimens, with an initial porosity of $\xi_0 = 0.32-0.33$, were prepared. All tests were performed with displacement controlled axial loading. Additional details of the test device and measurements of relevant parameters are provided in Han and Drescher (1993). The data for

mobilized friction reported by Han and Drescher (1993) is re-plotted as μ versus γ^p and fitted using the proposed evolution equation (Eqs. (19) and (20)) as shown in Fig. 3.

The heterogeneous porosity and fabric anisotropy of granular materials are known to affect the mobilized friction coefficient. Therefore, the formulation presented above is modified to account for these characteristics.

3.3.1. Effect of porosity heterogeneity on mobilized friction

High-degree of heterogeneity in the porosity, ξ = (void volume/total volume), distribution within the representative volume element (RVE) in granular materials is shown in Fig. 4. The use of simple homogenized values such as average porosity will not be sufficient to capture this variation. Assume that the actual distribution of the porosity $\xi(x)$ is known at the microscopic level (the particle length scale) at every material point,

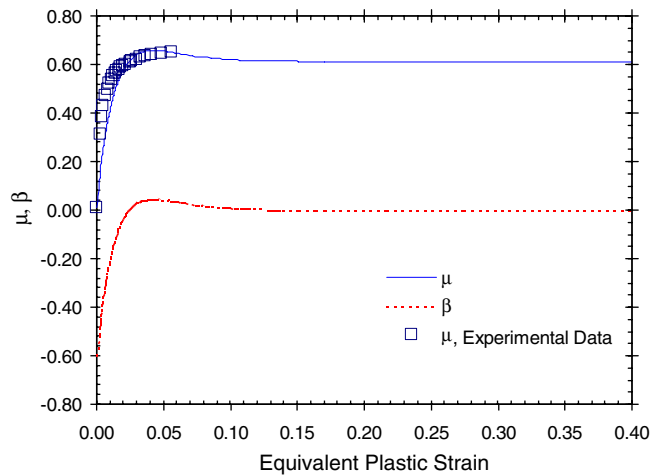


Fig. 3. Fitted mobilized friction evolution equation from experimental data of Han and Drescher (1993).

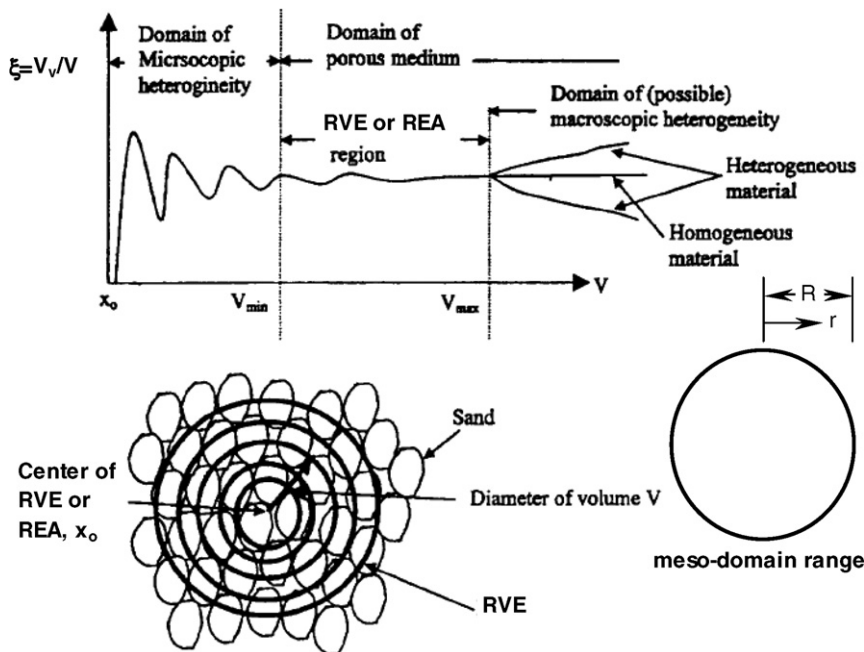


Fig. 4. Variation of porosity in neighborhood of point as function of averaging volume (modified after Bachmat and Bear, 1985).

and since the scale of the RVE is a few orders of magnitude higher than the particle length scale. Therefore, the RVE scale can be defined as a mesoscale for the continuum description of granular materials. Consequently, the average porosity over a meso-domain located at position x can be given as (Abramowitz and Stegun, 1965; Zbib, 1994; Vardoulakis and Sulem, 1995):

$$\bar{\xi}(x) = \frac{1}{V} \int_V g(x-r)\xi(r) dV \tag{21}$$

where $(R-r)$ defines the size of the meso-domain (Fig. 4), $g(x-r)$ is a probability distribution (density) function and V is the weighted volume. By expanding $\xi(r)$ around x we obtain:

$$\begin{aligned} \xi(r) = & \xi(x) + \nabla \xi \cdot (r-x) + \frac{1}{2!} \nabla^{(2)} \xi : (r-x) \otimes (r-x) \\ & + \frac{1}{3!} \nabla^{(3)} \xi : (r-x) \otimes (r-x) \otimes (r-x) + \frac{1}{4!} \nabla^{(4)} \xi : (r-x) \dots \end{aligned} \tag{22}$$

Substituting Eq. (22) into 21 and setting $r=0$ results in:

$$\bar{\xi}(x) = \xi(x) + a_1 \nabla^2 \xi(x) + a_2 \nabla^4 \xi(x) + \dots \tag{23}$$

with a_1, a_2, \dots being explicit functions of the size of the RVE (meso-domain). Note that because of spherical symmetry, the average porosity does not involve odd order gradients. Limiting the terms up to a second order for simplicity, Eq. (23) reduces to:

$$\bar{\xi}(x) = \xi(x) + a_1 \nabla^2 \xi(x) \tag{23a}$$

Thus, the addition of the Laplacian term in effect captures the deviation of porosity from its homogenous state in the meso-domain, i.e., it is a measure of the heterogeneity.

Neglecting the volumetric elastic deformation, the evolution of porosity is governed by mass conservation as (Vardoulakis and Sulem, 1995):

$$\dot{\xi} = (1 - \xi) \cdot D_{kk}^p \tag{24}$$

The formulation is now completed by assuming the mobilized friction coefficient to be a function of the second order gradient of porosity and, consequently, rewriting Eq. (19) as:

$$\mu(\gamma^p, \xi) = \mu_c + x_1 \left(\gamma^p + \frac{\mu_0 - \mu_c}{x_1} \right) \exp(-x_2 \gamma^p) \tag{25}$$

where μ_c is evaluated by:

$$\mu_c = \mu_{cv} (1.0 + a_3 (\xi_{crit} - (\xi_m + a_1 \nabla^2 \xi_m))) \quad (\text{for } \xi < \xi_{crit}) \tag{25a}$$

or by:

$$\mu_c = \mu_{cv} \quad (\text{for } \xi \geq \xi_{crit}) \tag{25b}$$

ξ_m and ξ_{crit} are the mean porosity (the porosity at $x=0$) and the critical porosity, respectively. a_3 is an additional material parameter. When it equals zero the above reduces to its homogeneous form (Eq. (19)).

3.3.2. Effect of fabric anisotropy on mobilized friction

The directional distribution of porosity $\xi(v) = \xi(\vartheta, \eta)$ within an REV can be approximated by (Kanatani, 1984; Pietruszczak and Krucinski, 1989a,b; Muhunthan et al., 1996).

$$\xi(v) = \xi_m (1 + \Omega_{ij} v_i v_j) \tag{26}$$

where, the components of the unit vector v are given by $v_1 = \sin \vartheta \sin \eta$, $v_2 = \cos \vartheta$, and $v_3 = \sin \vartheta \cos \eta$. The angles ϑ and η are shown in Fig. 5. The “mean porosity”, ξ_m , and the “fabric tensor”, Ω_{ij} , are given respectively by:

$$\xi_m = \frac{1}{4\pi} \int \xi(v) dv \tag{27}$$

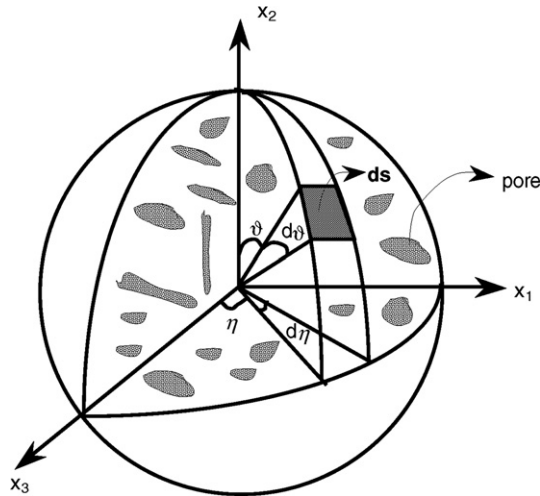


Fig. 5. Spherical coordinate system for a representative volume element.

and,

$$\Omega_{ij} = \frac{15}{2}(\psi_{ij} - \frac{1}{3}\delta_{ij}) \tag{28}$$

with the second moment tensor ψ_{ij} (Kanatani, 1984):

$$\psi_{ij} = \frac{1}{4\pi\xi_m} \int v_i v_j \xi(v) dv \tag{29}$$

Note that when the components of the fabric tensors are zero, Eq. (26) reduces to its isotropic form with mean porosity. Thus, the fabric tensor is a measure of the anisotropic distribution of porosity.

Fabric effects are incorporated into the multi-slip formulation by assuming the porosity in the mobilized friction to be directional. Consequently, $\mu(\gamma^p, \xi)$ becomes $\mu(\gamma^p, \xi_m, \Omega_{ij})$.

Since the fabric tensor Ω_{ij} is deviatoric (Eq. (28)), it is possible to represent its rate of change with deviatoric plastic stretching, d_{ij}^p , using an isotropic tensor valued functional representation (Boehler, 1987):

$$\dot{\Omega}_{ij} = \dot{\Omega}_{ij}(\Omega_{kl}, d_{ij}^p, \xi_m) \tag{30}$$

The functional form is generally complex. However, if the principal axes of d_{ij}^p and Ω_{ij} are assumed to be coincident, the relation can be modeled as (Muhunthan et al., 1996):

$$\dot{\Omega}_{ij} = \lambda d_{ij}^p \tag{31}$$

with:

$$\lambda = a_4(\xi_m) + a_5(\xi_m)\Omega_{ik}\Omega_{ki} \tag{31a}$$

where a_4 and a_5 are scalar functions of the mean porosity. The formulation is now completed by rewriting the mobilized friction as:

$$\mu(\gamma^p, \xi_m, \Omega_{ij}) = \mu(\gamma^p, \lambda) \tag{32}$$

Thus, Eqs. (25a) and (25b) can be modified to:

$$\mu_c = \mu_{cv}(1 + a_6 \cdot \lambda) \quad (\text{for } \xi < \xi_{crit}) \tag{32a}$$

or:

$$\mu_c = \mu_{cv} \quad (\text{for } \xi \geq \xi_{crit}) \tag{32b}$$

where a_6 is a material constant. Note that if a_6 equals zero the form in Eq. (32a) reduces to the isotropic case.

4. Shear band characteristics

The multi-slip gradient plasticity formulation has been implemented in ABAQUS (2003) as a User Material subroutine (designated as UMAT) for the case of two conjugate slip systems. The double-slip gradient model was used to study the characteristics of strain localization and shear band initiation in a biaxial test.

The biaxial test has been modeled using a plane strain finite element analysis. All analyses were carried out using four-node plane strain elements with reduced integration (designated in ABAQUS as CPE4R). The total number of mesh elements was varied in order to study the effect of strain localization and shear band on mesh sensitivity. The lower boundary of the mesh is assumed to be rigid. Simulations were carried out to ensure that localization characteristics were not affected by the friction imposed along the rigid boundary for the aspect ratio (height/width) of 3.5 used here (see also Albert and Rudnicki, 2001).

In the first phase, a confining pressure was applied to consolidate the specimen isotropically. Thereafter, axial compression was applied by increasing the vertical displacement on the top of the specimen. Based on the characteristics of the sand and the test conditions, the following material constants were used in the gradient multi-slip model:

- elastic properties: stiffness modulus (E) = 180 MN/m², poisson ratio (ν) = 0.2,
- mobilized friction function (Eq. (19), Fig. 3): initial mobilized friction (μ_o) = 0.01; constant volume friction (μ_{cv}) = 0.61; $x_1 = 25.0$; $x_2 = 55.0$,
- critical porosity of the sand, $\zeta_{crit} = 0.43$,
- active slip systems initial orientation $\zeta_1 = \pi/4 + \phi/2$ and $\zeta_2 = -\pi/4 - \phi/2$ where ϕ is the mobilized friction angle of the sand at failure measured in the experiment, $\phi = 31.5^\circ$ was used.

The complete force displacement curve predicted by the FE analysis is compared with the test observation as shown in Fig. 6. It can be seen that the model here leads to good predictions regardless of the differing mesh sizes used. However, the use of the finer mesh provided better convergence of the results. The final deformed shapes of the FE mesh are as shown in Fig. 7. It can be seen that deformation localizes into a narrow shear band whether a weak element is present (Fig. 7b) or not (Figs. 7a and c). The introduction of a weak element is achieved here by using reduced values of constant volume friction (μ_{cv}) (Fig. 7b). It can also be seen that shear band characteristics is very much dependent on the initial slip system (cf. Fig. 7a and c) and on the location of the weak element (Fig. 7b). The inclination of the resulting shear band with the introduction of weak elements

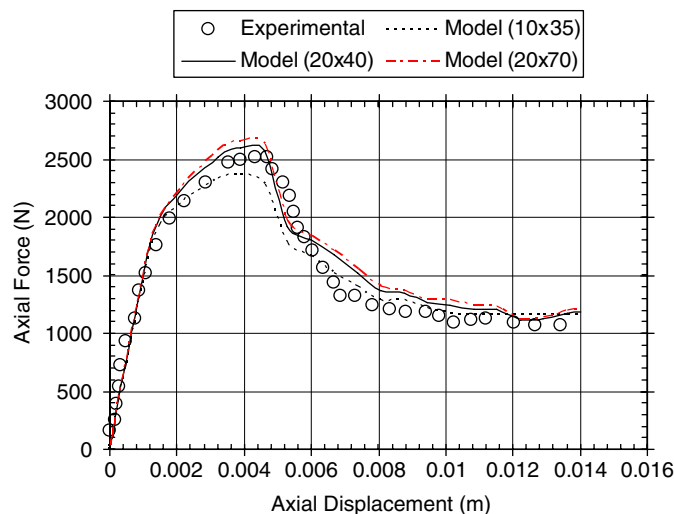


Fig. 6. Force displacement curve for $\zeta_1 = \pi/4 + \phi/2$, $\zeta_2 = -\pi/4 - \phi/2$, a_3 and $a_6 = 0.0$, experimental data of Han and Drescher (1993).

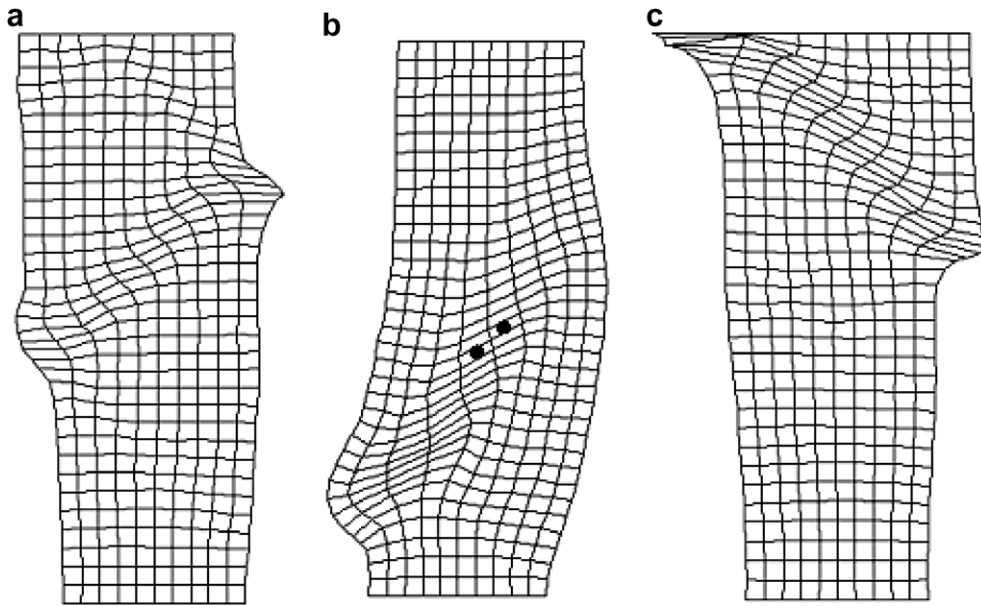


Fig. 7. Deformed shapes of 10×35 elements, a_3 and $a_6 = 0.0$ (a) $\zeta_1 = \pi/4 + \phi/2, \zeta_2 = -\pi/4 - \phi/2$ (b) $\zeta_1 = \pi/4 + \phi/2$ and $\zeta_2 = -\pi/4 + \phi/2$ with weak element seeded (shown as a dot) (c) $\zeta_1 = \pi/4 + \phi/2, \zeta_2 = -\pi/4 - 0.45 \cdot \phi/2$.

in the central portion of the mesh was measured to be $53^\circ \pm 2^\circ$ relative to the minor principal stress axis (Fig. 7b). The experimentally measured angle was found to vary between 55° and 56° for confining pressure of 200 kPa (Han and Drescher, 1993).

The variation of the orientation angle between shear bands and the direction of minor principal stress is shown in Fig. 8 as a function of different initial slip systems. The shear band inclination angles vary essentially between 48° and 60.5° depending on the initial slip system arrangement. On the basis of force equilibrium and Coulomb’s theory the theoretical inclination of the shear band orientation angle is found to be $\theta = \pi/4 + \phi/2$. The upper limit of the results obtained here correspond to this angle ($\phi = 31.5^\circ$). Roscoe (1970) suggested that

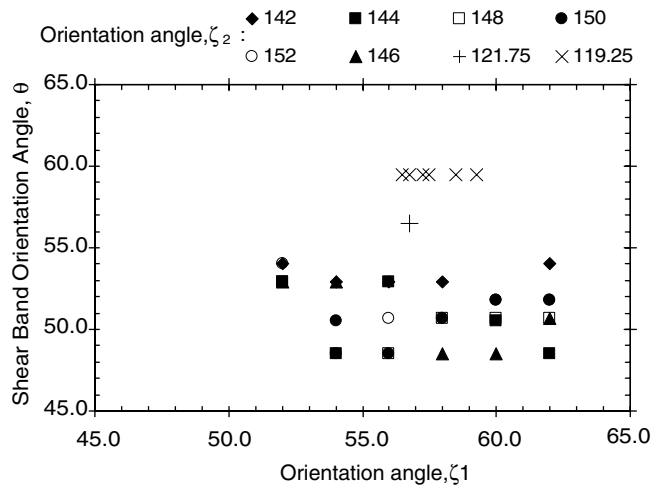


Fig. 8. Shear band orientation with different initial slip system (symbols denote the inclination angle of the second slip system).

the friction angle in Coulomb’s orientation must be replaced with the angle of dilation ψ , i.e., $\theta = \pi/4 + \psi/2$. The lower limit of the results here corresponds to this value. Arthur et al. (1977) found that shear bands were inclined between the Coulomb and Roscoe directions and proposed that the average of the two angles $\theta = \pi/4 + (\psi + \phi)/4$ be used to define the orientation. Theoretical analyses by Vardoulakis (1980) supported this latter orientation. Examination of the results here show that a majority of the orientation angles lie between Roscoe’s and Arthur’s directions. Numerical analysis conducted by Vermeer (1990) shows that shear band inclination in plane strain tests is limited between the Coulomb and Roscoe directions and that the actual inclination is very sensitive to the boundary conditions imposed. Here, we have essentially found the same observation based on the use of different initial slip systems but with the same boundary conditions. Experimental measurements of shear band orientations on Santa Monica Beach sand reported by Lade (2003) and Lade and Wang (2001) show them to locate between locate Coulomb and Arthur inclination. Further, their results show that the shear band orientation in dense sands to favor the Coulomb direction. The above discussion suggests that shear band orientation is complex and that it depends on initial slip system, packing density, and boundary conditions.

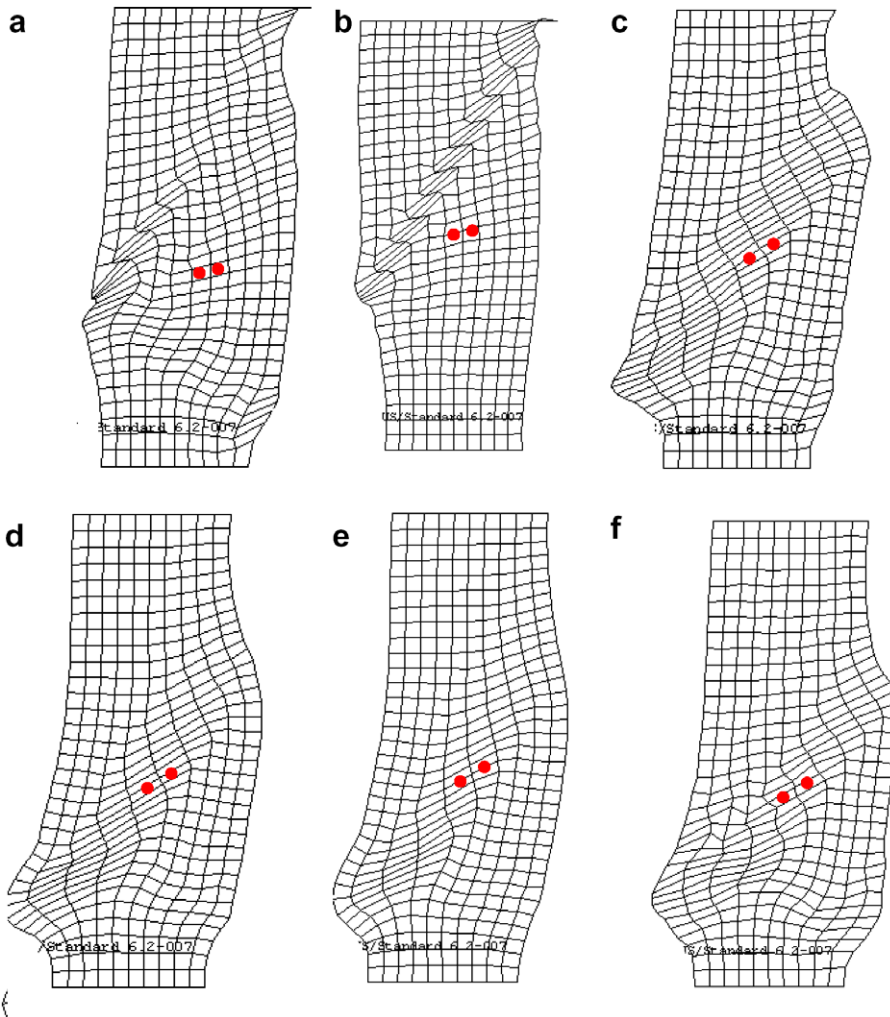


Fig. 9. Effect of non orthogonal conjugate slip system on the pattern of the deformation with weak element seeded (shown as a dot) (a) $\zeta_1 = 58.00^\circ$, $\zeta_2 = 145.25^\circ$, (b) $\zeta_1 = 58.25^\circ$, $\zeta_2 = 145.5^\circ$, (c) $\zeta_1 = 59.00^\circ$, $\zeta_2 = 146.00^\circ$, (d) $\zeta_1 = 60.0^\circ$, $\zeta_2 = 149.25^\circ$ (e) $\zeta_1 = 60.75^\circ$, $\zeta_2 = 150.75^\circ$, (f) $\zeta_1 = 58.75^\circ$, $\zeta_2 = 148.75^\circ$.

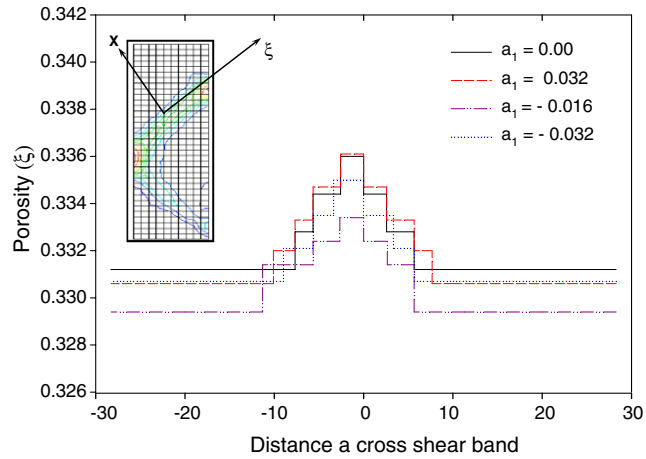


Fig. 10. Diffusion of porosity concentration on the shear band, $a_3 = 0.335$.

The effects of the non-orthogonality of the initial slip systems on shear band characteristics are as shown in Fig. 9. It can be seen that slight deviations from orthogonality would lead to changes in the location of the shear band in spite of the weak elements being kept at the same location within the specimen.

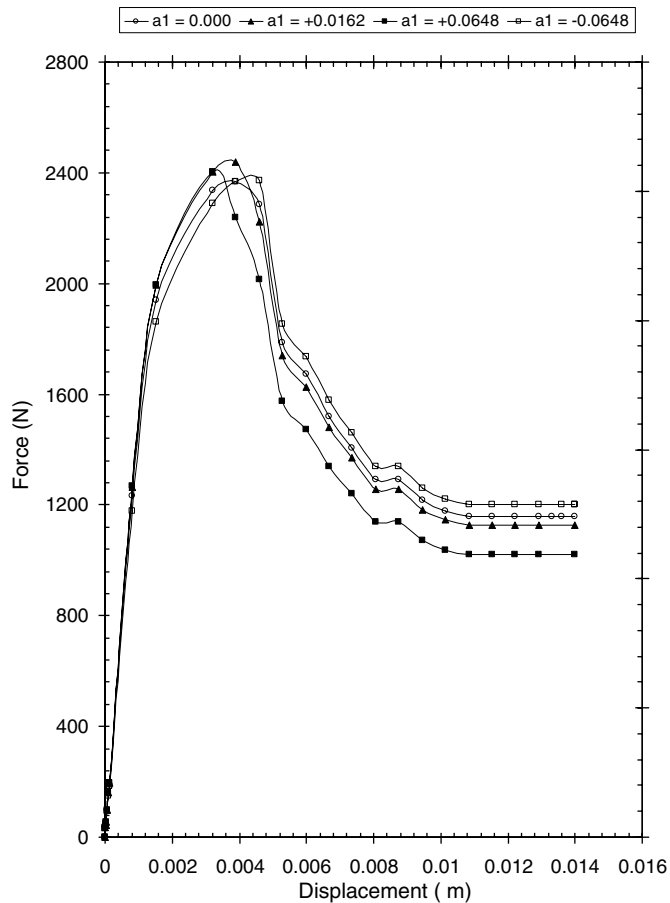


























Fig. 11. Effect of gradient coefficient, a_1 in axial force axial displacement curve, $a_3 = 0.335$.

Table 1
Summary of the experimental results on shear band localization (Desrues and Viggiani, 2004)

Test	γ_0 (kN/m ³)	e_0	σ'_3 (kPa)	H_0/L_0	Lubrication (Y/N)	End plates (L/R/TT) ^a	Observed localization	'imperfections'
SH00	15.75	0.650	80	2.00	N	L		
Shf00	14.93	0.741	90	2.00	Y	L		
shf01	14.93	0.741	90	2.00	Y	L		
shf02	13.68	0.900	85	2.20	N	R		
shf03	14.05	0.850	90	2.20	Y	L		
shf04	13.68	0.900	80	3.60	N	L		
shf05	15.65	0.661	80	2.00	Y	L		
shf06	15.65	0.661	80	2.00	Y	R		Left tilting 
shf07	15.65	0.661	80	2.00	Y	L		Right tilting 
shf08	15.65	0.661	80	2.00	Y	R		
shf09	15.65	0.661	80	2.00	Y	L		
shf10	15.65	0.661	80	2.00	Y	L		Soft inclusion
shf11	15.47	0.680	80	2.00	Y	L		Hard inclusion
shf12	15.65	0.661	80	2.00	Y	TT		Lateral load

(continued on next page)

Table 1 (continued)

Test	γ_0 (kN/m ³)	e_0	σ'_3 (kPa)	H_0/L_0	Lubrication (Y/N)	End plates (L/R/TT) ^a	Observed localization	'imperfections'
shf13	15.65	0.661	80	2.00	Y	L		
shf14	15.65	0.661	80	3.55	Y	L		
shf15	15.65	0.661	80	3.55	Y	L		
shf16	15.65	0.661	80	3.55	N	L		
shf17	15.65	0.661	80	2.00	N	L		
shf18	15.65	0.661	80	3.55	N	L		
shf19	15.65	0.661	80	3.55	Y	R + TT		
shf20	13.97	0.860	80	2.00	Y	R + TT		

^a L, both platens locked, i.e., prevented from rotating and translating in the horizontal direction; R, both platens allowed to rotate without translating; TT, top platen free to translate in the horizontal direction, but not to rotate, while the bottom platen is locked in place.

One of the features of strain localization is the sharp variation of porosity across the shear band (Fig. 10). Therefore, the resulting higher gradients in the porosity need to be taken into account to properly account for modeling the post localization behavior in granular materials. The gradient term in the mobilized friction accounts for this phenomenon here and its performance depends on the values of parameter a_1 . The effect of parameter a_1 (Eq. (25a)) on localization was studied using a fixed mesh size of (10×35) . It can be seen that a_1 diffuses the concentration of the porosity within the shear band by making it more uniform across the localized region (Fig. 10). Further, its use affects the post peak strain-softening segment of the load displacement curve as shown in Fig. 11. The negative values of a_1 lead to a decrease in the strain softening effect whereas the opposite is true in the case of positive values of a_1 . This is mainly because a negative value of a_1 will generate an increase in μ_c (Eq. (25)). This in turn would lead to an increase in the post peak value of the mobilized friction and the strengthening the granular material.

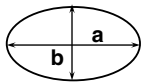
Desrues and Viggiani (2004) have summarized experimental evidence on plane strain tests which suggests the shear band characteristics to be very much dependent on test arrangement and conditions of the specimen (Table 1). It is also worth noting that shear bands occur with or without the inclusions (cf. Table 1 and Fig. 7). Since the directionality of the porosity depends on the porosity fabric tensor, it was decided to use some data on photo elastic measurements of initial fabric for samples reported by Oda et al. (1985) in biaxial shear tests.

The specimens consisted of circular and oval shaped particles deposited at different angles. From the reported photo elastic measurements of Oda et al. (1985) the porosity distribution was calculated by Muhunthan (1991) using a stereological procedure. The corresponding values for the porosity fabric tensor Ω_{ij} are as shown in Table 2. These values are used to study the influence of initial fabric on the localization in biaxial shear tests.

The deformed model configurations for the different deposition angle and particle shapes are as shown in Fig. 12. It can be seen that the localization of deformation into shear band is dependent very much on the type of particle shape as well as the depositional angle. In circular shaped particles, the deformation does not appear to localize into a defined shear band whereas in oval shaped particles it does so. Furthermore, such localization is very much dependent on the angle of deposition as well as the shape of the particles. Thus, the use of fabric tensor may enable the quantification of shear bands and their orientation in granular materials.

Table 2
Void fabric tensor measurements on biaxial test (Muhunthan, 1991)

Case No.	Particle shape/deposition angle, ^a θ_d	Ω_{11}	Ω_{12}	Ω_{22}
I	Circular, $\theta_d = 0^\circ$	1.32	-0.03	-1.32
II	Oval I, $\theta_d = 0^\circ$	0.53	-0.08	-0.53
III	Oval II, $\theta_d = 0^\circ$	-0.04	0.07	0.04
IV	Oval II, $\theta_d = 60^\circ$	0.86	0.16	-0.86
V	Oval II, $\theta_d = 90^\circ$	0.54	0.09	-0.54



Oval I: $a/b=1.1/1.0$
Oval II: $a/b=1.4/1.0$

^a Deposited with respect to the horizontal bedding plane.

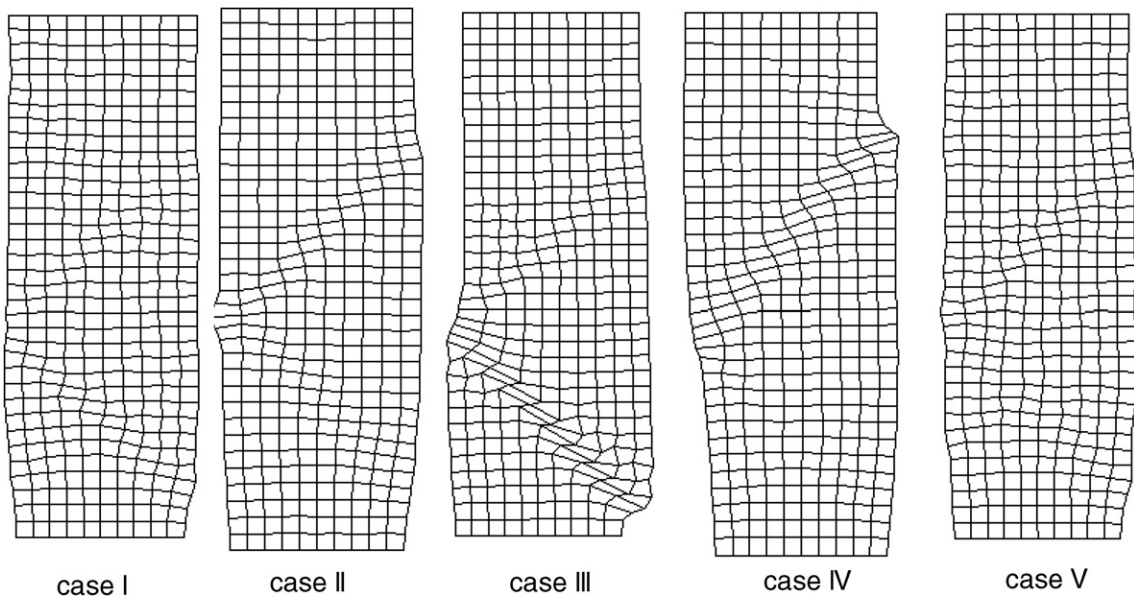


Fig. 12. Deformation shape for a mesh with 10×35 elements for ideal particle shapes, $a_4, a_5,$ and $a_6 = 0.33, 0.0648,$ and $0.0175, \zeta_1 = \pi/4 + \phi/2$ and $\zeta_2 = -\pi/4 - \phi/2$ (see Table 2 for case legend).

5. Conclusions

A multi-slip gradient formulation is presented in this paper to model strain localization in granular materials. The double slip version of the model has been incorporated into a finite element code and used to simulate plane strain test results on dry sand. The effects of granular microstructure have been accounted for by assuming the mobilized friction to be a function of either porosity gradient or the use of fabric tensor measure. Based on the analysis reported, the following conclusions can be drawn:

- (a) The presence of weak element shifts the location and orientation of the shear band; however, it has nothing to do with the presence/occurrence of strain localization.
- (b) Strain localization and shear band characteristics are highly dependent on the initial slip system of the granular materials.
- (c) The shear band orientation angle is bounded by $\theta = \pi/4 + \psi/2$ (Roscoe) and $\theta = \pi/4 + \phi/2$ (Coulomb). The specific location of the orientation angle within these bounds, however, is the result of a combination of complex interaction among initial slip system, packing density, and boundary conditions.
- (d) Sharp variation of porosity is found across the shear band with a pronounced peak along the midsection. The use of gradient term diffuses the porosity concentration within shear band and decreases the softening effect on the post peak load displacement curve.
- (e) Localization of deformation into shear band is dependent very much on the type of particle shape as well as the depositional angle. In circular shaped particles, the deformation does not appear to localize into a defined shear band whereas in oval shaped particles it does so.

It is noted that we had taken a bold step to construct a continuum theory macroscopically with explicit consideration of microstructure bypassing the intermediate step of constructing a microscopic theory for each individual phenomenon such as granular dilatancy. The numerical implementation of the theory addresses directly the localization features of a continuum plasticity sand model with microstructure. Many of the parameters of the various models albeit physically based are determined here by curve fitting. Further analysis of these models preferably based on micromechanical considerations are needed to validate or improve upon the parameters as used here.

Acknowledgement

The study was sponsored by the National Science Foundation under the Grant CMS-0010124 to Washington State University. This support is gratefully acknowledged.

References

- ABAQUS, 2003. Hibbitt, Karlsson and Sorensen Inc, Pawtucket, RI.
- Abramowitz, M., Stegun, I.A., 1965. Handbook of Mathematical Functions. Dover, NY.
- Albert, R.A., Rudnicki, J.W., 2001. Finite element simulations of Tennessee marble under plane strain laboratory testing: effect of sample-platen friction on shear band onset. *Mech. Mater.* 33, 47–60.
- Al Hattamleh, O., 2003. Investigation of the deformation of granular materials: a micromechanics approach. Ph.D Thesis, Washington State University.
- Al Hattamleh, O., Muhunthan, B., Zbib, H.M., 2004. Gradient plasticity modeling of strain localization in granular materials. *Int. J. Numer. Anal. Methods Geomech.* 28 (6), 465–561.
- Anand, L., Gu, C., 2000. Granular materials: constitutive equations and strain localization. *Int. J. Mech. Phys. Solids* 48 (8), 1701–1733.
- Anand, L., 1983. Plane deformation of ideal granular materials. *J. Mech. Phys. Solids* 31, 105–122.
- Asaro, R.J., 1979. Geometrical effects in the inhomogeneous deformation of ductile single crystals. *Acta Metallurgica* 27 (3), 445–453.
- Arthur, J., Dunstan, T., Al-Ani, Q., Assadi, A., 1977. Plastic deformation and failure in granular media. *Geotechnique* 27 (1), 53–74.
- Balandran, B., Nemat-Nasser, S., 1993a. Double sliding model cyclic deformations of granular materials, including dilatancy effects. *Int. J. Mech. Phys. Solids* 41 (3), 573–612.
- Bathurst, R.J., Rothenburg, L., 1990. Observations on stress-force-fabric relationships in idealized Granular Materials. *Mech. Mater.* 9, 65–80.

- Bachmat, Y., Bear, J., 1985. On the concept and size of representative elementary volume. In: *Advances in Transport Phenomena in Porous Media*, Proceeding of the NATO Advanced Study Institute, Conducted at Newyark, Martinus Nijhoff Publishers, DE, 1987, pp. 3–20.
- Boehler, J.P. (Ed.), 1987. *Application of Tensor Functions in Solid Mechanics*. Springer Verlag, New York.
- Chang, C.S., Hicher, P.Y., 2005. An elasto-plastic model for granular materials with microstructural consideration. *Int. J. Solids Struct.* 42 (14), 4258–4277.
- de Borst, R., Muhlhaus, H.B., 1992. Gradient dependent plasticity: formulation and algorithmic aspects. *Int. J. Numer. Methods Eng.* 35 (3), 521–539.
- Desrues, J., Viggiani, G., 2004. Strain localization in sand: an overview of the experimental results obtained in Grenoble using stereophotogrammetry. *Int. J. Numer. Anal. Methods Geomech.* 28 (4), 279–321.
- Engelen, R.A.B., Fleck, N.A., Peerlings, R.H.J., Geers, M.G.D., 2006. An evaluation of higher-order plasticity theories for predicting size effects and localization. *Int. J. Solids Struct.* 43 (7–8), 1857–1877.
- Gajo, A., Bigoni, A.D., Wood, D.M., 2004. Multiple shear band development and related instabilities in granular materials. *J. Mech. Phys. Solids* 52 (12), 2683–2724.
- Han, C., Drescher, A., 1993. Shear bands in biaxial tests on dry coarse sand. *Soils Foundations* 33, 118–132.
- Huang, Y., Qu, S., Hwang, K.C., Li, M., Gao, H., 2004. A conventional theory of mechanism-based strain gradient plasticity. *Int. J. Plast.* 20 (4–5), 753–782.
- Hirth, J.P., 1992. *Theory of Dislocations*, second ed. Krieger Pub. Co., Malabar, FL.
- Kachanov, M., Sevostianov, I., 2005. On quantitative characterization of microstructures and effective properties. *Int. J. Solids Struct.* 42 (2), 309–336.
- Kanatani, K., 1984. Stereological determination of structural anisotropy. *Int. J. Eng. Sci.* 24 (2), 207–222.
- Lade, P., 2003. Analysis and prediction of shear banding under 3D conditions in granular materials. *Soils Foundations* 43 (4), 161–172.
- Lade, P., Wang, Q., 2001. Analysis of shear banding in true triaxial tests on sand. *J. Eng. Mech., ASCE* 127 (8), 762–768.
- Liu, X., Scarpas, A., Blaauwendraad, J., 2005. Numerical modelling of nonlinear response of soil. Part 2. Strain localization investigation on sand. *Int. J. Solids Struct.* 42 (7), 1883–1907.
- Mehrabadi, M.M., Cowin, S.C., 1978. Initial planar deformation of dilatant granular materials. *J. Mech. Phys. Solids* 26, 269–284.
- Mehrabadi, M.M., Nemat-Nasser, S., Oda, M., 1982. On statistical description of stress and fabric in granular materials. *Int. J. Numer. Anal. Meth. Geomech.* 6, 95–98.
- Muhunthan, B., 1991. *A micromechanics of steady state, collapse and stress strain modeling of soils*. Ph.D. Thesis, Purdue University.
- Muhunthan, B., Chameau, J.L., Masad, E., 1996. Fabric effects on the yield behavior of soils. *Soils Foundations JSGE* 36 (3), 85–97.
- Nemat-Nasser, S.A., 2000. Micromechanically based constitutive model for frictional deformation of granular materials. *Int. J. Mech. Phys. Solids* 48, 1463–1541.
- Nemat-Nasser, S., Zhang, J., 2002. Constitutive relations for cohesionless frictional granular materials. *Int. J. Plast.* 18 (2002), 531–547.
- Oda, M., Konishi, J., Nemat-Nasser, S., 1982. Experimental micromechanical evaluation of strength of granular materials: Effect of particle rolling. *Mech. Mater.* 1, 267–283.
- Oda, M., Nemat-Nasser, S., Konishi, J., 1985. Stress-induced anisotropy in granular masses. *Soils Foundations* 25 (3), 85–97.
- Oda, M., Kazama, H., Konishi, J., 1998. Effects of induced anisotropy on the development of shear bands in granular materials. *Mech. Mater.* 28 (1–4), 103–111.
- Oka, F., Higo, Y., Kimoto, S., 2002. Effect of dilatancy on the strain localization of water-saturated elasto-viscoplastic soil. *Int. J. Solids Struct.* 39 (13–14), 3625–3647.
- Pietruszczak, S., Krucinski, D., 1989a. Description of anisotropic response of clays using a tensorial measure of structural disorder. *Mech. Mater.* 8, 237–249.
- Pietruszczak, S., Krucinski, D., 1989b. Considerations on soil response to the rotation of principal stress directions. *Comput. Geotech.* 8, 89–110.
- Roscoe, k., 1970. The influence of strains in soil mechanics. *Geotechnique* 20 (2), 129–170.
- Rudnicki, J.W., Rice, J.R., 1975. Conditions for the localization of deformation in pressure sensitive dilatant materials. *J. Mech. Phys. Solids* 23, 371–394.
- Shizawa, K., Zbib, H.M., 1999. A thermodynamical theory of gradient elastoplasticity with dislocation density tensor. I: Fundamentals. *Int. J. Plast.* 5 (9), 899–938.
- Spencer, A.J.M., 1964. A theory of the kinematics of ideal soils under plane strain condition. *J. Mech. Phys. Solids* 12, 337–351.
- Spencer, A.J.M., 2003. Double-shearing theory applied to instability and strain localization in granular materials. *J. Eng. Math.* 45 (1), 55–74.
- Taylor, D.W., 1948. *Fundamentals of Soil Mechanics*. Wiley, New York.
- Tobita, Y., 1989. Fabric tensors in constitutive equations for granular materials. *Soils Foundations* 29 (4), 99–104.
- Vardoulakis, I., 1980. Shear band inclination and shear modulus in biaxial tests. *Int. J. Numer. Anal. Methods Geomech.* 4, 103–119.
- Vardoulakis, I., Sulem, J., 1995. *Bifurcation Analysis in Geomechanics*. Blackie Academic, Glasgow.
- Vardoulakis, I., 1996. Deformation of water-saturated sand: I. uniform undrained deformation and shear banding. *Geotechnique* 46 (3), 441–456.
- Vermeer, P.A., 1990. The orientation of shear bands in biaxial tests. *Geotechnique* 40 (2), 223–236.

- Zbib, H.M., Aifantis, E.C., 1989. A gradient-dependent flow theory of plasticity: application to metal and soil instabilities. *J. Appl. Mech. Rev.*, ASME 42 (11, 2), 295–304.
- Zbib, H.M., 1991. On the mechanics of large inelastic deformations: noncoaxiality, axial effects in torsion and localization. *Acta Mechanica* 87, 179–196.
- Zbib, H.M., 1993. On the mechanics of large inelastic deformations; kinematics and constitutive modeling. *Acta Mechanica* 96, 119–138.
- Zbib, H.M., 1994. Size effects and shear banding in viscoplasticity with kinematic hardening. In: Batra, R.C., Zbib H.M. (Eds.), *International Mechanical Engineering Congress and Exposition*, pp. 19–33.